Production Engineering (2024) 18:233–251
https://doi.org/10.1007/s11740-023-01244-0

MATERIAL PROPERTIES

A process-reliable tailoring of subsurface properties during cryogenic turning using dynamic process control

Berend Denkena[1] · Bernd Breidenstein[1] · Hans Jürgen Maier[2] · Vannila Prasanthan[1] · Lara Vivian Fricke[2] · Felix Zender[1] · Hai Nam Nguyen[1] · Stefan Zwoch[2] · Marcel Wichmann[1] · Sebastian Barton[2]

Received: 30 August 2023 / Accepted: 14 November 2023 / Published online: 20 December 2023

Abstract
Considering the current demands for resource conservation and energy efficiency, innovative machining concepts and increased process reliability have a significant role to play. A combination of martensitic hardening of the subsurface and near-net-shape manufacturing represent a great potential to produce components with wear-resistant subsurfaces in an energy- and time-saving way. Within the scope of the present study, the influence of cryogenic machining of metastable austenitic steel on the martensitic transformation and surface quality was investigated. Different cooling strategies were used. A soft sensor based on eddy current in-process measurements was used to determine and subsequently affect the martensitic transformation of the subsurface. The feed rate and component temperature were identified as significant factors influencing the martensitic transformation. However, a high feed rate leads to an increase in surface roughness, and thus to a reduction in component quality. For this reason, a roughing process for achieving maximum martensitic transformation was carried out first in the present study and then a reduction in the surface roughness by maintaining the martensitic subsurface content was aimed for by a subsequent finishing process. With the knowledge generated, a dynamic process control was finally set up for designing the turning process of a required subsurface condition and surface quality.

Keywords Cryogenic turning · Subsurface properties · Dynamic process control · Deformation-induced martensitic transformation · Eddy-current sensor

1 Introduction

The subsurface condition is a crucial factor for the properties of components that are under vibrational, tribological, and corrosive loads [1]. The targeted use of robustly adjusted subsurface properties in manufacturing processes, therefore, leads to improved component service life and reliability. Especially in manufacturing processes, such as turning, which are often the final process steps, control of the final surface and subsurface properties is crucial. Today,

✉ Vannila Prasanthan
prasanthan@ifw.uni-hannover.de

Berend Denkena
denkena@ifw.uni-hannover.de

Bernd Breidenstein
breidenstein@ifw.uni-hannover.de

Hans Jürgen Maier
maier@iw.uni-hannover.de

Lara Vivian Fricke
fricke@iw.uni-hannover.de

Felix Zender
zender@ifw.uni-hannover.de

Hai Nam Nguyen
nguyen@ifw.uni-hannover.de

Stefan Zwoch
zwoch@iw.uni-hannover.de

Marcel Wichmann
wichmann@ifw.uni-hannover.de

Sebastian Barton
barton@iw.uni-hannover.de

[1] Institute of Production Engineering and Machine Tools, Leibniz University Hannover, An der Universität 2, 30823 Garbsen, Germany

[2] Institut für Werkstoffkunde (Materials Science), Leibniz University Hannover, An der Universität 2, 30823 Garbsen, Germany

however, the conditioning of surfaces and subsurfaces during the final machining process of metal components is still not completely understood [2, 3].

The joint control of geometry and surface properties, which has not been possible so far, is expected to lead to a paradigm shift in manufacturing technology [2]. Hence, one important scientific challenge is to develop a deeper understanding of the underlying mechanisms that lead to a modification of subsurface properties while machining [1]. By knowing the underlying mechanisms, it might be possible to tailor the subsurface microstructure of metal components directly within the machining process. For example, in order to withstand high mechanical and tribological loads, components must have high core ductility and a hard subsurface. It is, therefore, important to create a predefined hardened subsurface as part of the manufacturing process. Most often, a suitable microstructure is created in the subsurface by heat treatment processes prior to machining the part. However, this is often not possible with austenitic steels due to their low carbon content [4]. In addition, these processes consume time and energy, while also distorting the part. This requires an additional process to restore the part geometry. Hence, not requiring a heat treatment to create a hardened subsurface would be highly advantageous.

Frölich et al. have shown that the wear of a cryogenically-turned metastable austenitic steel is slightly higher than that of a carburized steel [5]. Their study shows that it is possible to produce austenitic steels with hardened substrates by cryogenic turning. Since the robustness of the process, with regard to the desired setting of the substrate, is not yet known, an in-process, non-destructive testing method would be helpful to be able to reliably produce the desired microstructure of the subsurface [3]. By linking novel sensor technology with process knowledge of soft sensors, previously immeasurable variables become measurable in the process for the first time [2].

The martensite content, for example, influences the hardness of the surface. It is a variable which cannot be measured directly in the process. By integrating these newly determinable variables by the developed soft sensor into a dynamic process control, the robustness of the process with regard to the generation of defined subsurface conditions can be significantly increased. By this, the dynamic process control reacts to observable disturbance variables, such as the starting material conditions. In this study, an eddy current testing system, a non-destructive, electromagnetic method, is used as basis for an in-process soft sensor to detect the martensitic transformation of the subsurface hardening during cryogenic turning [6–9]. An eddy current testing sensor creates a primary magnetic field that induces eddy currents in electrically conductive materials. These eddy currents create a secondary magnetic field that overlaps with the primary magnetic field. The resulting magnetic field can be measured using a measuring coil, within which a voltage is induced and analyzed. The induced voltage is influenced by the material properties, like the electrical conductivity and magnetic permeability. Additonally, contrary to austenite, α'-martensite is ferromagnetic. To analyze the change in the magnetic properties, the analysis of higher harmonics is used in the present study. Further details regarding this testing method can be found in Ref. [7].

Moreover, in previous investigations the influence of process parameters and different tool microgeometry, like cutting edge rounding and flank face modification, on martensite transformation was analyzed [10]. Based on this, different model approaches have been investigated to model the correlation between process parameters and martensite content. With an inverse modeling approach, the link to achieve desired martensite contents by using specific process parameters was created [11]. Therefore, if necessary, the setting variables can be adjusted during processing. This soft sensor will be able to ensure the desired subsurface microstructure, and thus the properties of the manufactured components, even in the presence of observable disturbances. Such disturbances can be semi-finished product tolerances, the tool setting angle, the initial tool wear condition, and machine vibration, or hidden disturbances, such as tool wear or chipping and scattering material properties. Additionally, due to variation in the alloy composition, there is an influence from the batch used [12]. Therefore, in order to ensure the desired subsurface properties despite batch variations and process disturbances, a dynamic process control would be advantageous.

In many studies, it has been found that an increasing feed leads to an increased martensite subsurface content [10, 13, 14]. However, a high feed rate leads to an increase in surface roughness, and thus to a reduction in component quality [15, 16]. For this reason, a roughing process for maximum martensitic transformation was first carried out in the present study, then a reduction of the surface roughness, by maintaining the martensitic subsurface content, was sought in a subsequent finishing process. Hotz et al. have previously discovered that when using a CO_2 in-process cooling, a second arbitration process can even lead to an increased martensite subsurface content [17]. In the present study, different cooling strategy combinations of CO_2 in-process cooling and a pre-cooling use of liquid nitrogen (LN_2) are analyzed. This is motivated from a previous study, see Ref. [18], where it was found that a sub-zero metalworking fluid, developed by Ref. [19, 20], and a pre-cooling LN_2 cooling leads to an enhanced martensitic transformation.

2 Project overview

To further explain the developed soft sensor, a broader overview of the present project will be given in this section. The overall goal of this project, as part of the priority programme

2086, is to develop a methodology for the reliable adjustment of subsurface properties during machining with an adaptive manufacturing system.

The hypothesis for the methodology is that a process-safe adjustment of subsurface properties can only be achieved by supervising the production of each individual component. This requires an in-process sensor system that monitors the workpiece, while also supplying measurement data during production. This measurement data is compared with process-parallelly generated simulation data to detect deviations from the ideal manufacturing conditions. Simulation and test engineering are combined into an adaptive model so that the manufacturing system is able to react immediately and autonomously by changing the process parameters to ensure consistent subsurface properties.

Process-reliable setting of subsurface properties can only be realized if it is also possible to map the relevant machining conditions within the machining process. For this purpose, a material removal simulation is necessary, which makes it possible to compare the data obtained by the sensors with the simulation, thus showing the deviations between the set machining conditions and the actual machining conditions in the process. These differences can then be used to control the process. Furthermore, it is necessary to develop a robust sensor technology that is capable of detecting changes in the subsurface properties under the conditions prevailing in the machine tool. Eddy current technology was used for this purpose. If correlated correctly, this technology provides direct information about the machined component subsurface [7, 8].

Metastable austenitic steels, in which phase transformations can be induced in the subsurface by a cryogenic machining process, offer a particularly interesting field of research. These materials provide increased hardness and wear resistance of the components, which conventionally can only be achieved through additional surface hardening. At the same time, process-parallel material removal simulation [6, 21] and conventional sensor technology are used to collect the data required to describe the interrelationships between the resulting subsurface properties and the process parameters, on the one hand and the cutting edge microgeometry on the other. This data serves as the basis for a database. This database is further expanded by all of the data obtained in the laboratory from the starting material and the machined material, by the new eddy current testing technology, after the process has been qualified for it. Together, all of the data is used to teach a machine model that can predict the phase transformations in the subsurface. The new testing technique was ultimately integrated into a machine tool and used, together with the learned model, to investigate the change of the subsurface properties during the process. Through this, both the model and the testing technique were validated.

Furthermore, a dynamic feed forward control system had to be developed in order to reliably adjust the subsurface properties in the machining of steels by means of deformation-induced austenite-martensite transformation. The control concept of the dynamic feed forward control will be given in section 4.6. Due to the previously identified strong influence of the local material temperature on the austenite-martensite transformation [14, 18, 19], a new cryogenic cooling strategy was implemented.

The planned overall system is based on a multi-stage turning process. The martensite content in the subsurface is adjusted through a roughing process with high feed rates. However, the required high feed rates will lead to a decrease in surface quality. For this reason, a finishing process is carried out at the end of the turning process in order to achieve a high surface quality. By means of the cooling strategy design, using the dynamic feed forward control, the finishing process can be adapted using the martensite content and geometry data determined in the roughing process. If there is a deviation between the nominal and actual subsurface state, the individual roughing processes and the finishing process can be adapted based on the measurement data acquired during planning. A combination of cooling, roughing, and finishing processes appears to be a suitable process strategy.

3 Materials and methods

3.1 Material

The experiments were conducted using an 1.4301, which is a metastable austenitic steel. It was solution annealed at 1050 °C for 45 min and slowly cooled in the furnace to obtain a homogeneous microstructure without any ferromagnetic phases. The alloying composition was measured using spark spectroscopy and the mass fraction amounts to 0.035 % C, 0.38 % Si, 2.0 % Mn, 18.39 % Cr, 0.238 % Mo, 8.16 % Ni, and 0.086 % N and Fe balance.

3.2 Eddy current testing

Eddy current testing was performed inside the machine tool in real-time, i.e., in situ by using an in-house built system. The test frequency was 800 Hz and the excitation current amounted to 2 A. The strength of the excitation magnetic field, directly at the sensor tip, was 3.5 kA/m. A detailed set-up can be found in Ref. [11].

3.3 Metallography

The metallographic images were acquired with an optical microscope (Leica digital microscope, DM4000M). The specimens were first polished, then etched. The samples

were etched with Beraha II (distilled water, hydrochloric acid, ammonium hydrogen difluoride).

Micro-hardness measurements were conducted on polished cross-sections using a Q10 A+ by Qness with a load force of 100 gf (HV0.1), for a loading time of 10 s, in the depth range from 50 µm to 600 µm in 50 µm steps, in the middle of the samples.

3.4 Production of chip roots

Since the chip formation can give important information on the cutting process, and hence subsurface modification, a chip analysis of the cryogenic turning process was carried out. The chip roots were obtained using a modified Split Hopkinson test rig. Details of the modification can be found in Ref. [22]. Hereby, the temperatures were set by emerging the samples into liquid nitrogen before the mechanical test. After shooting the cutting specimens along the cutting edges, chip roots remained in the surface. The experiments were conducted at room temperature, -45 °C and -110 °C. Afterwards, the chip roots were mounted, polished, and then etched using Beraha II.

3.5 Temperature analysis with moving heat source

The workpiece temperature during machining significantly influences martensite formation. Knowledge of the temperature distribution inside the component is crucial for understanding its impact on martensite formation throughout the component depth. However, measuring this distribution requires extensive experimental efforts, necessitating the use of simulation methods. In this study, the commercial software Ansys 2019 R3 was employed to simulate the temperature distribution inside the workpiece. The simplified schematic configuration of the simulation is shown in Fig. 1.

The simulation utilized a thermally-transient model, initially assuming a Gaussian heat source with a cylindrical shape. A stainless steel shaft with a diameter of 47 mm and a machining length of L = 60 mm were considered analogous to the experimental investigations. The convective and radiative boundary conditions are included in this model, with a heat transfer coefficient of $1.44 \cdot 10^{-2}$ W/(mm^2·K) as well as radiation between the component surface and surrounding area. The following assumptions were made for the simulation: (1) The thermal conductivity was assumed to be constant over temperature. (2) The workpiece material is homogeneous and isotropic. (3) The change of the phase is not taken into account. The moving heat source is Gaussian distributed and is defined as follows:

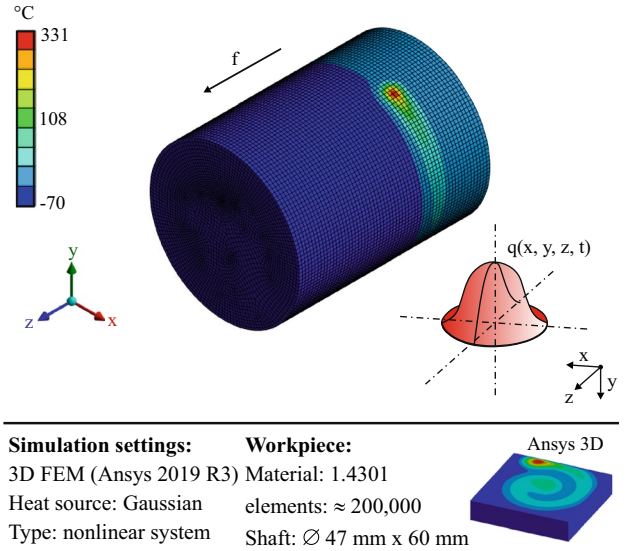

Fig. 1 Simulation setup with moving heat source

$$q(x,y,z,t) = q_{\max} \cdot \exp\left(\frac{-3 \cdot (x - \zeta \cdot \cos(t \cdot v_r))^2}{r^2} + \frac{(y - \zeta \cdot \sin(t \cdot v_c))^2 + (z - f \cdot t)^2}{r^2}\right) \quad (1)$$

with q_{max}: maximum heat flux at the center of the heat spot, ζ: radius of the beam, v_r: velocity in circumferential direction, f: feed in z direction and r: radius of the Gaussian heat source.

The aim of the simulation in the first step is to show, on the one hand, basic qualitative correlations between the nozzle diameter and the temperature distribution inside the component. On the other hand, an understanding of the temperature distribution in the shear zone, with prior nitrogen cooling during cutting engagement, while turning, is to be generated. In future work, it will then be necessary to combine the two simulation approaches with a moving heat source (analogy to the heat induced by the cutting tool) and a cold source (analogy to the CO_2 in-process cooling), dependending on the initial temperature of the component.

3.6 Hardware concept and experimental setup

The cryogenic longitudinal turning investigations and the implementation of the process control were carried out on a turnmill center DMG Mori NTX1000 with additional turret for simultaneous machining. On this machine the hardware concept shown in Figure 2 was implemented. During the investigations, the tool spindle was used to mount the eddy current sensor for in-situ measurements of the martensite content. Additionally, a nozzle was mounted in order to provide in-process CO_2 cooling. For

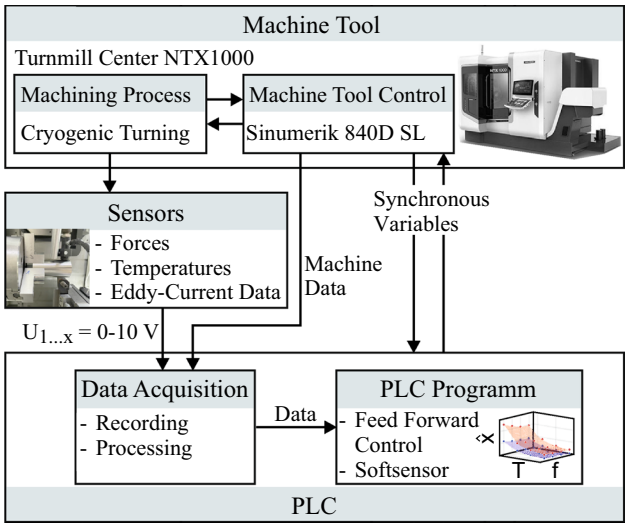

Fig. 2 Hardware concept

the actual turning process, the turret was used, while the process forces were measured by a Kistler 9129 dynamometer. Furthermore, the turret was used to mount a thermocouple type K for temperature measurement before the process. The data measured by the thermocouple, the dynamometer, and the eddy current sensor, were transferred to a Beckhoff PLC as analog voltage signals. The PLC was also connected via a PROFIBUS interface to the Siemens Sinumerik 840D SL of the machine. This connection allows a collection of the axis data of the machine and interaction with the process running on the machine tool by synchronous variables.

The experimental investigations for the modeling and inverse modeling were conducted using uncoated indexable inserts (CNMA120408 by Kennametal). The material of the inserts consists of tungsten carbide cobalt (K68). The process parameters feed f, depth of cut a_p, cutting speed v_c and initial workpiece temperature T are each varied in two factor levels: f is varied at 0.3 mm and 0.7 mm, a_p at 0.2 mm and 0.5 mm, v_c at 30 m/min and 70 m/min and T at -70 °C and -110 °C. The experiments were performed in a full factorial manner. They were further extended varying just f and T since those process parameters have the highest effect on the martensite formation. Further experiments with five different levels for f (from 0.1 mm to 0.5 mm) and six different levels for T (from -150 °C to -50 °C) were then conducted full factorially. The workpieces have a diameter of 49.7 mm and a length of 50 mm. The experiments with the varying cooling strategies were conducted with a CNMG120412-SM1 by Sandvik. The used process parameters were: f = 0.1 mm and f = 0.4 mm, v_c = 100 m/min, T = -72 °C and T = 22 °C

3.7 Modeling and inverse modeling approach

Modeling the correlation between the process parameters and the subsurface properties is necessary in the first step for setting the subsurface. Based on this, an inverse modeling approach allows the determination of necessary process parameters by combining the model with a meta-heuristic used for solving optimization problems. For the modeling approach of martensite, the Adaboost regressor was chosen. The cross validation method with five runs was used for modeling, resulting in a distribution of training to test data in the ratio of 80 % to 20 %. In this case, the data set was divided into five random blocks and one block was used as a test data set to check the trained model for overfitting based on the training data of the remaining blocks. This was done five times with different combinations, so each block was used once as a test data set. The implementation was done with the python library Scikit-learn. For the multi-criteria optimization, the genetic algorithm (GA) is used. It is suitable for multi-criteria problems and the solution tends not to remain in a local optimum because of random mutations in the iterative process for finding the optimal solution. The GA is linked with the prediction models of martensite and surface roughness. For the surface roughness, the linear regression was used.

4 Results and discussion

4.1 Results of in-process eddy current measurements

The higher the amplitude of the 1st and the 3rd harmonic was, the higher is the newly generated subsurface martensite content. A correlation between the eddy current signals and the martensite content, determined by reference measurements, was created in Ref. [9]. In Fig. 3, the amplitude of the 1st and the 3rd harmonic of in situ eddy current testing measurements are shown. Here, only an in-process CO_2 cooling was applied. Two roughing steps were conducted, using a feed of f = 0.4 mm. The amplitudes of both harmonics increased in the second turning step, meaning that more martensite was created. This is comparable to the findings by Hotz et al. [17]. The longer the process duration, the more cooling lubricant is applied, and thereby the cooler the workpiece becomes. Further, the lower the temperature was, the lower is the stacking fault energy. A low stacking fault energy promotes the deformation-induced martensitic transformation [23, 24]. Hence, more martensite is produced in the second turning step [7, 14, 17, 22].

In Fig. 4, the results of a two-step turning process are shown. Here, a roughing and a finishing process step were conducted. Comparing Fig. 4 a) and b), it can be seen that

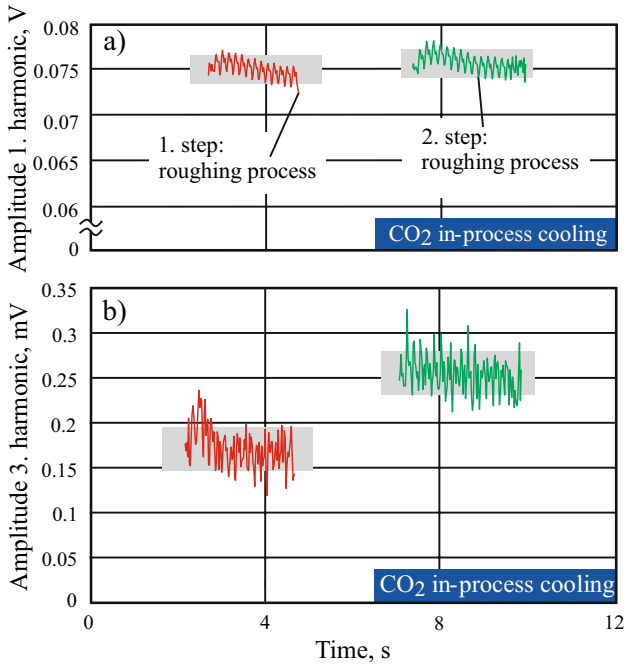

Fig. 3 in situ eddy current testing with CO_2 in-process cooling, two subsequent roughing steps a) amplitude of the 1st harmonic, b) amplitude of the 3rd harmonic

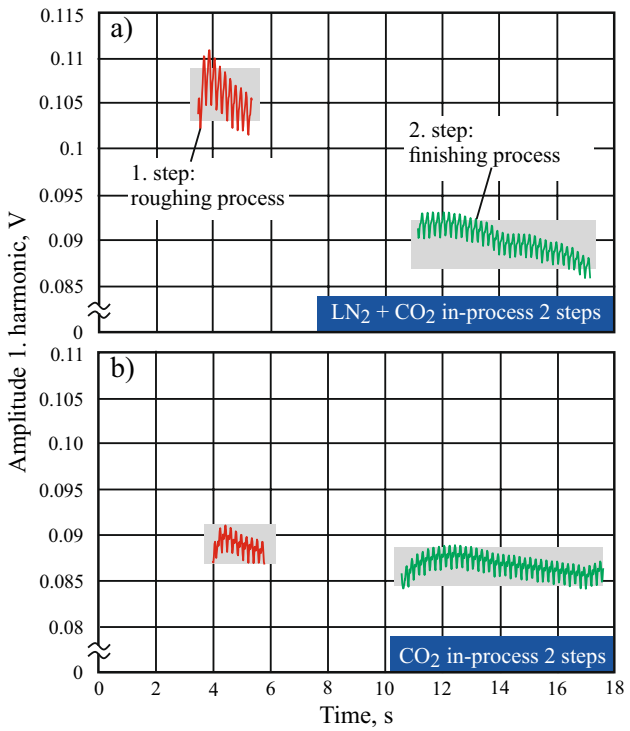

Fig. 4 in situ eddy current testing amplitude of the 1st harmonic a) pre-cooling using LN_2 and CO_2 in-process cooling, two subsequent turning steps, b) CO_2 in-process cooling, two subsequent turning steps

the amplitude of the 1st harmonic of eddy current testing is higher when using a LN_2 pre-cooling, see 4 a). A sufficient cooling effect is achieved [18]. The cutting parameters were kept constant for the experiments shown in Fig. 4 a) and b). First, a roughing process was conducted. Subsequently, a finishing process step was applied. The amplitude level of the 1st harmonic of eddy current testing is lower in the second step when compared to the first one, if an LN_2 pre-cooling is used. When only an in-process CO_2 cooling was used, the amplitude level of the 1st harmonic of eddy current testing is similar in the second turning step compared to the first one. This means when using solely an in-process CO_2 cooling, which also results in higher workpiece temperatures in the first cutting step compared to LN_2 pre-cooling, after the second turning step, a similar subsurface martensite content is gained. Here again, it is suspected that the workpiece is colder in the second turning step than in the first one. Even though the cutting feed is lower in the finishing step, the lower workpiece temperature leads to a similar martensitic transformation rate. However, unlike Hotz et al. [17] where only an in-process cooling was applied, no increase in the subsurface martensite content was detected, see Fig. 4 b).

Figure 5 again shows the amplitude of the 1st harmonic of eddy current testing for in-process measurements. As in Fig. 4, it can be seen that the amplitude of the 1st harmonic is higher when a pre-cooling is applied and more martensite is produced in the subsurface. However, when comparing the combination of in-process CO_2 cooling and LN_2 pre-cooling, a more stable progress can be seen than for the one without

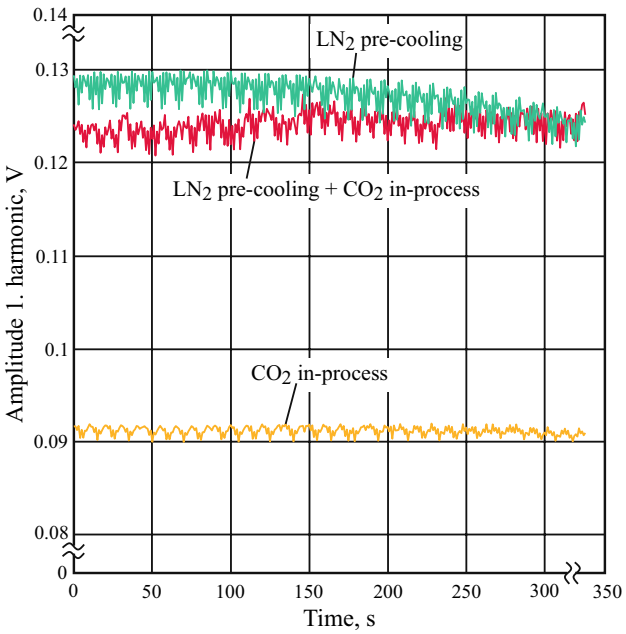

Fig. 5 Comparison of in situ eddy current testing amplitude of the 1st harmonic for different cooling concepts

in-process CO_2 cooling. For longer turning times, the pre-cooled workpieces heated up, and thus less martensite is produced. If an in-process cooling is applied, the sample remains cold and a homogeneous martensite subsurface content can be produced over the sample length. The validity of this assumption was proven by random temperature measurements. It was observed that a shaft, pre-cooled with LN_2, reaches a final temperature of T = -48 °C after turning, while a shaft with in-process CO_2 cooling had a final temperature of T = -10 °C, and a shaft with a combination of both cooling strategies (LN_2 pre-cooling and in-process CO_2 cooling) reached a final temperature of T = -59 °C. In conclusion, as also described in Ref. [18], a pre-cooling leads to the highest possible martensite subsurface content. However, an in-process cooling is necessary if longer workpieces are machined, so that a homogeneous martensite subsurface content can be produced over the whole workpiece length. Otherwise, the workpiece warms up and less martensite is induced at the end of the machining process.

4.2 Metallographic examination of deformation-induced martensitic transformation

As it can be seen in Fig. 4 a), if the workpiece is pre-cooled using LN_2, less martensite can be found in the subsurface after the subsequent finishing step, when compared to the roughing step. Without an in-process cooling, the workpiece temperature is increased in the second turning step, as well as a smaller feed being applied. This leads to a less pronounced deformation-induced martensitic transformation.

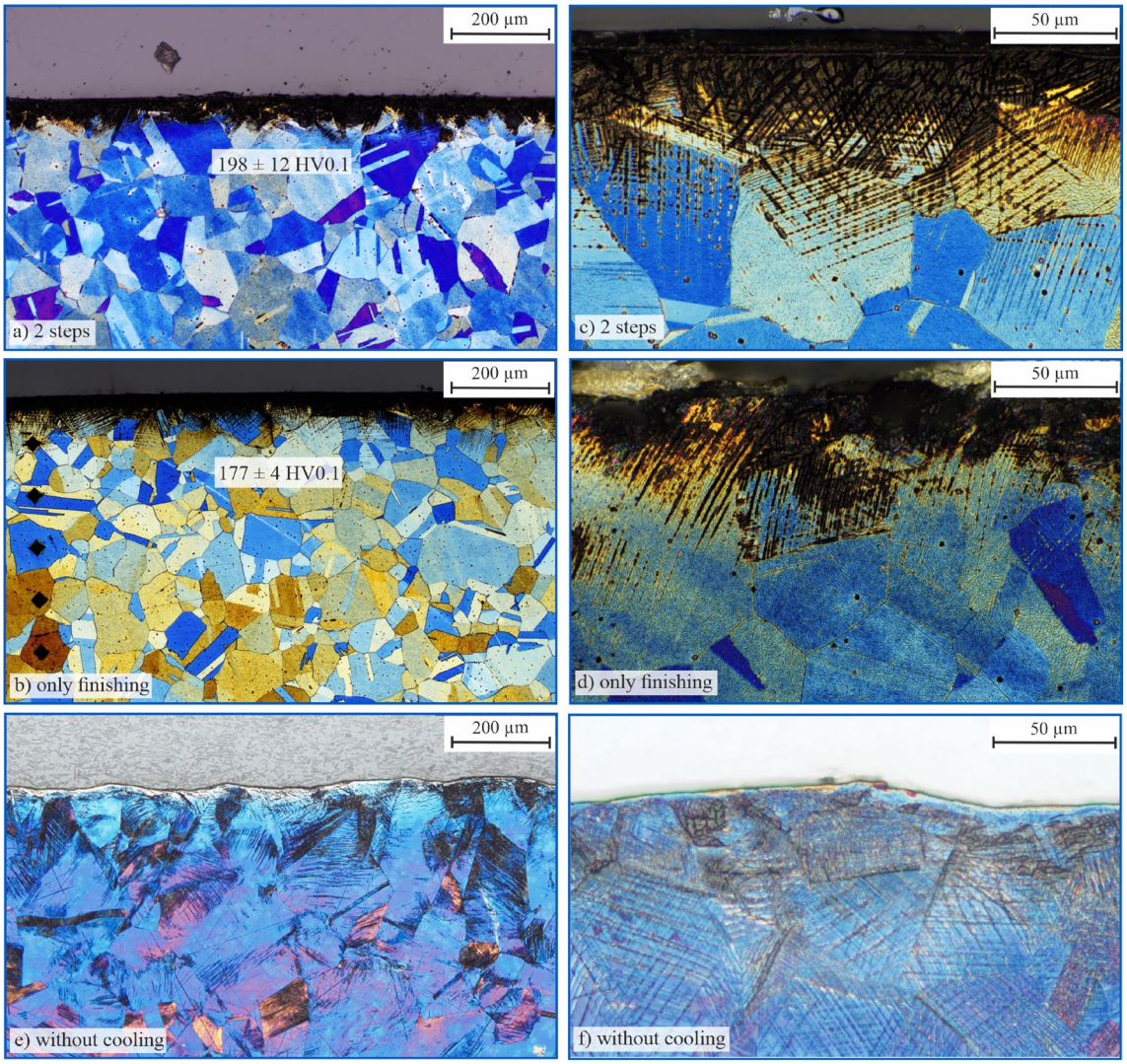

Fig. 6 Metallographic pictures of the newly created subsurfaces of LN_2 and in-process CO_2 cooling a + c) two-step turning process b + d) only finishing step e + f) machining without cooling. The hardness was measured at a depth of 70 μm below the surface

In Fig. 6, metallographic cross-sections of a two-step, a) + c), and an one-step turning process, b) + d), are shown. The black areas are deformed areas where martensite might have been created [22, 25]. More black areas, and therefore likely more martensite, are created if a roughing step is applied, compare Fig. 6 c) and d). However, a hardening compared to the base material (150 HV0.1) can also be achieved if only a cryogenic finishing process with low cutting feeds is applied.

In addition to the newly created surface using a Split Hopkinson test rig, see chapter 3.4, an analysis of chip roots, created using different cutting conditions, was possible. In Fig. 7 a–c chip roots produced at three different cutting temperatures are shown.

At room temperature, Fig. 7a, deformed black areas interspersed with colored areas can be seen. The colored areas are austenitic. That means only a little martensite was created since austenitic grains are still present within the chip. Compared to Fig. 7a, in Fig. 7b segregated, completely black areas are obvious. A segmented chip formation is visible. Between the black, deformed areas, colored stripes appear. Here, due to the shearing, and therefore heat generation, the austenite did not transform into martensite.

Compared to Fig. 7b, the colored austenitic areas in the segmented chip are smaller and less pronounced than in Fig. 7c. Due to the cutting temperature reduction, more martensite was generated within the chip. A more detailed view on the austenitic areas between the deformed areas can be seen in Fig. 8. Again, it is obvious that only a few black areas were produced at room temperature, Fig. 8a. The chip remains mostly austenitic. In Fig. 8b and c, the sheared austenitic microstructure in the segmented chip, between the deformed areas, is visible.

Moreover, in Fig. 7b and c bright white areas are obvious. In Fig. 7d, a magnification of one of the white areas is shown using less illumination. Very small, austenitic grains are visible. Hence, the appearance of the white areas is reminiscent of white etching layers. Such layers which can be found in the surface of martensitic, ferritic, or pearlitic steels after machining when high cutting speeds are used in conjunction with tool flank wear [26].In the present study, the emerging white etching layers seem to have a similar grain refinement as the white etching layers in martensitic, ferritic, or pearlitic steels. A further evaluation of the emerging white etching layers in austenitic steels was not conducted in this study but should be performed in future studies. Deep rolling can also lead to the formation of white etching layers due to the high strains in high carbon steels [27]. The white etching effect is often explained by a grain size reduction, typically between 30 and 500 nm, due to dynamic recrystallization within the turning process [26–29]. Until now, a white etching layer in an austenitic steel has not been described in the literature. However, the grain size reduction is accompanied

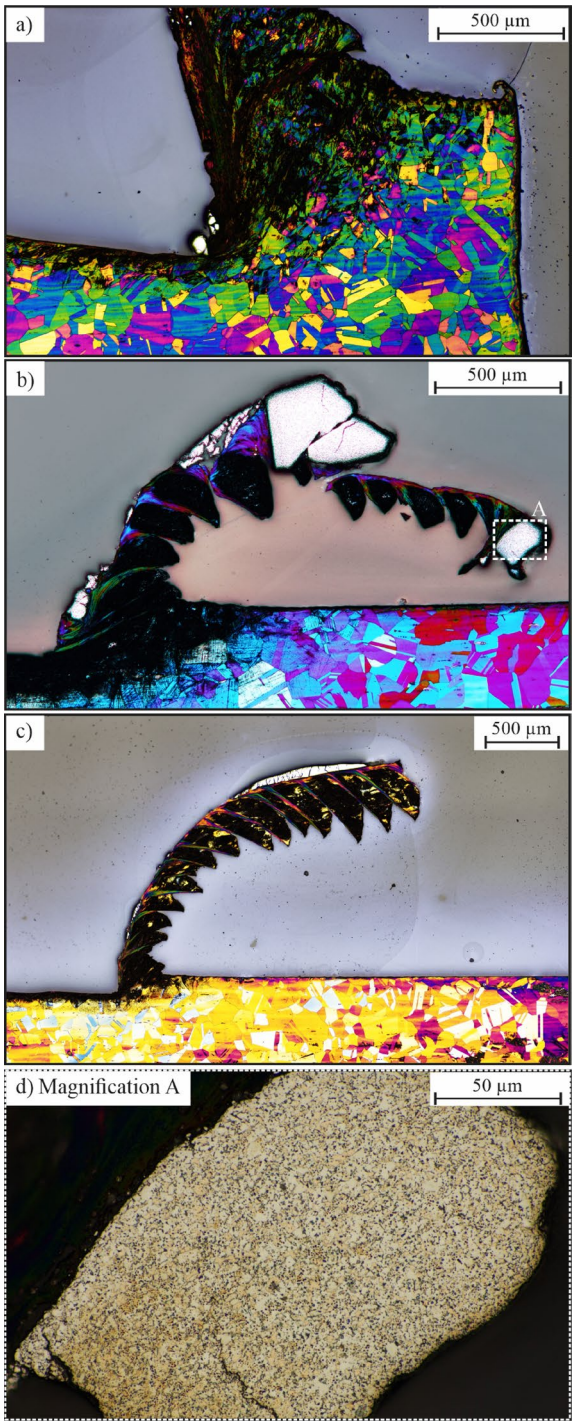

Fig. 7 Metallographic pictures of chip roots produced at **a** room temperature, **b** -45 °C and **c** -110 °C. **d** Detailed view of white etching area in **b**

with a hardness increase [26]. This is also the case in the white areas within the present study. In Fig. 9, hardness indentations within the chip root of Fig. 7b are presented. Compared to the base material, the hardness in the white areas is increased tenfold. Since greater hardness often is

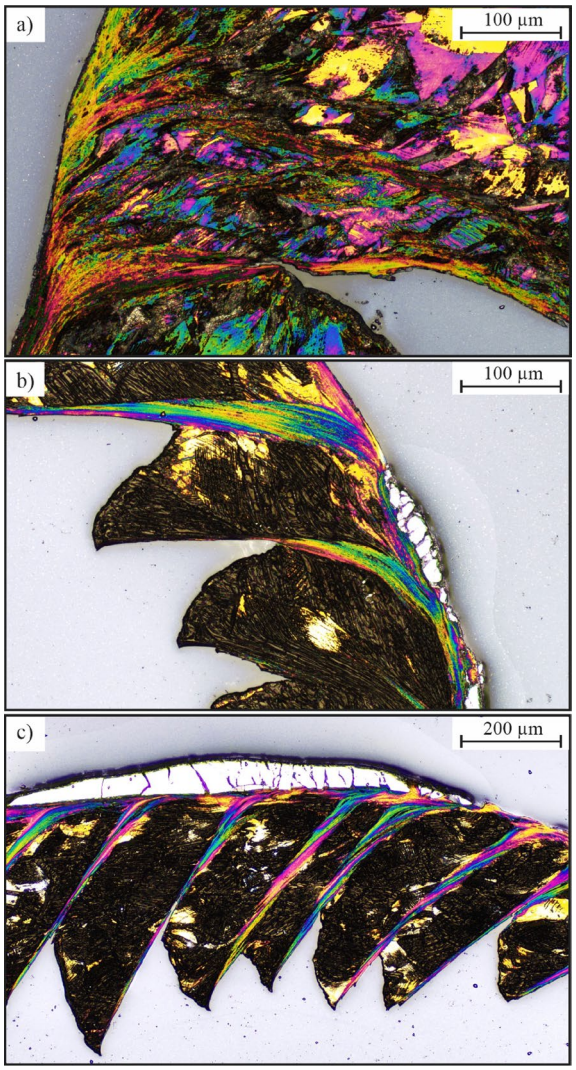

Fig. 8 Detailed metallographic pictures of chip roots produced at **a** room temperature, **b** -45 °C and **c** -110 °C

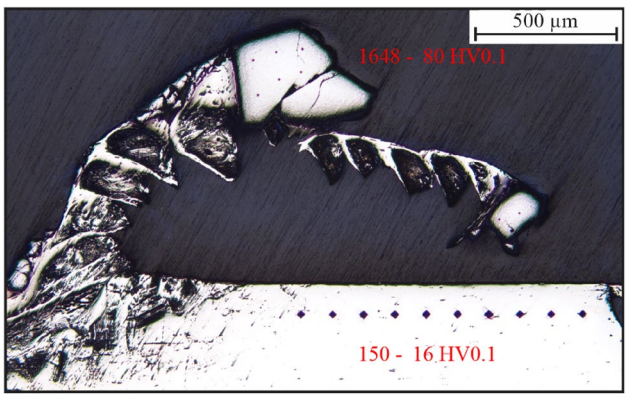

Fig. 9 Hardness measurements from white etching area and base material

accompanied by brittle behavior, white etching layers are unwanted in a subsurface after the turning process. However, the white etching layers have only been found within the chip and not in the newly created subsurface in the present study. Further studies should focus on the emergence mechanism of these white etching layers in the chips of metastable austenitic steels.

The microstructure of high carbon steels, where white etching layers often occur, is not austenitic. Here, due to the high temperatures within the cutting process, an austenitic phase transformation happens and retained austenite occurs. As a results of this and the dynamic recrystallisation, the grains are refined [28]. The differences in the composition of white layers are probably due to the fact that, depending on the application, different white layers are actually formed [30]. By analyzing the chip roots, it can be determined that the heat dissipation by the chip is sufficient for the LN_2 pre-cooling method. Further, in the present case, the base material is already austenitic and no phase transformation has to occur in order to produce a white etching layer.

4.3 Analysis of process forces and surface topography

In order to investigate and evaluate the influence of different cooling strategies on the mechanical load during both the roughing and the final finishing operations, force measurements were conducted. The effect of the cooling strategies CO_2 in-process cooling, pre-cooling with LN_2, and the combination of both, on process forces is depicted in Fig. 10.

For reference, force measurements without cooling were also conducted. In the roughing process, the passive force emerged as the most dominant force component, while during finishing, the cutting and passive forces were observed to be at a similar level. The literature [16, 31] has previously reported significant reductions in process forces by adjusting the process parameters for the finishing step, which is confirmed in this study as well. The cooling strategy demonstrates a considerable impact on the passive and cutting forces, while the feed force is only minimally affected. In particular, the LN_2 pre-cooling strategy displays a remarkable reduction in process forces when compared to other cooling strategies. This outcome may be attributed to the altered chip formation observed in Fig. 11, resulting from the pre-cooling process with LN_2.

The choice of cooling strategy has a profound influence on chip morphology. Without cooling, the observed chip formation consists of lamellae with comparatively less plastic deformation than the chips produced with cooling strategy, see Fig. 11a. In contrast, employing CO_2 in-process cooling (11b) preserves similar chip morphology, but with noticeably larger areas exhibiting possible martensitic transformation, as evident by the darkened regions in the microsections.

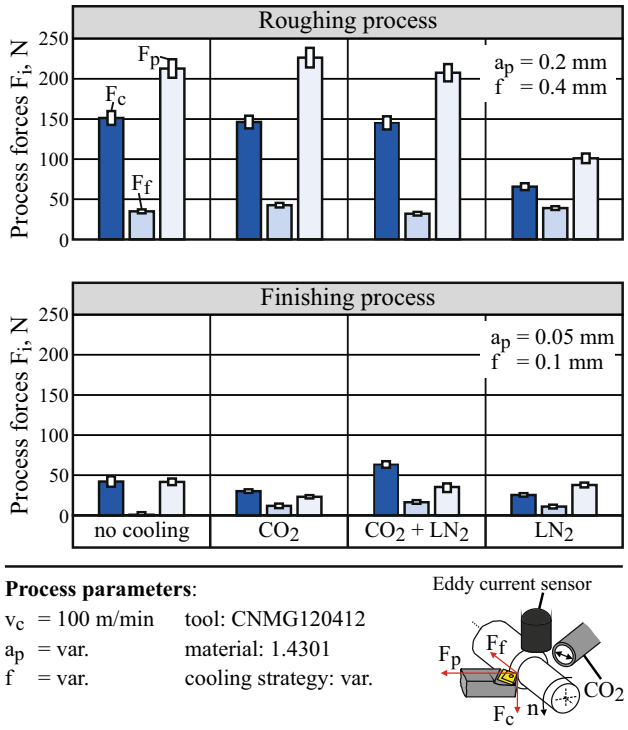

Fig. 10 Influence of different cooling strategies on process forces

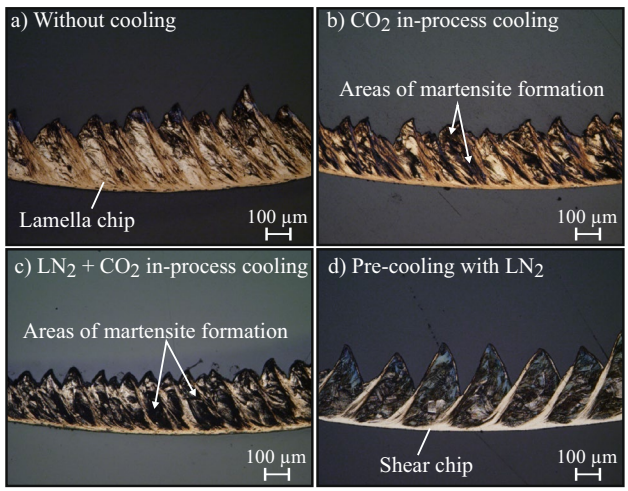

Fig. 11 Influence of different cooling strategies on chip formation

A prior LN_2 cooling process results in a significant transformation of the chip formation, see Figs. 11c and 11d. The formation of shearing chips with well-defined shear bands becomes apparent. The combination of LN_2 pre-cooling with in-process CO_2 cooling further enhances the frequency of chip formation. In both cases, there is a pronounced darkening of the microsections, indicating the occurence of martensitic phase transformations between the shear bands.

In-process CO_2 cooling leads to a more rapid cooling during the compression phase, resulting in an increased frequency of chip formation, i.e. leads to a reduction in the distance between the lamellae. The enhanced cooling rate promotes quicker sliding and shearing, thereby contributing to the observed changes in chip morphology and the martensitic phase transformations. The results demonstrate that a reduction in workpiece temperature significantly influences chip morphology, with LN_2 pre-cooling in particular playing a key role in inducing plastic deformation. This also explains the increased deformation-induced martensitic transformation for pre-cooled workpieces. Plastic deformation is needed as a nucleation site for the strain-induced martensitic transformation [32], which occurs in the present case. Additionally, the combination of in-process CO_2 cooling with nitrogen pre-cooling, enhances the frequency of chip formation.

The cooling process is a crucial aspect of turning operations, that impacts chip formation, tool wear, and process forces. These changes are used specifically to initiate the martensitic phase transformation. CO_2 in-process cooling, involving liquid CO_2 expansion through a nozzle, offers a promising cooling solution, see also Ref. [14, 19]. Therefore, in this study, one aim was to investigate the influence of nozzle diameter on process forces during the CO_2 in-process cooling in turning processes. The nozzle diameter was varied in three stages (8 mm, 10 mm, and 12 mm) to

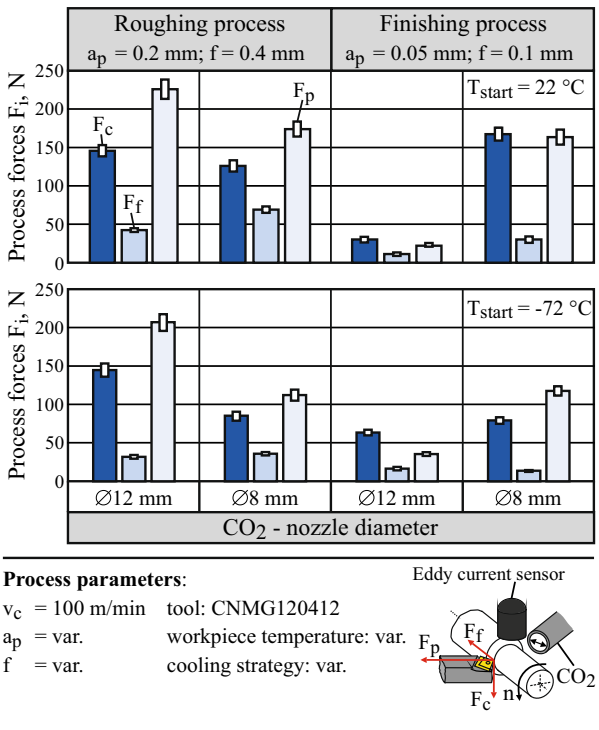

Fig. 12 Influence of the CO_2 nozzle diameter on the process forces in relation to the component temperature

analyze its effect on process forces. For better understanding, only the largest and smallest diameters are considered in Fig. 12. During roughing, increasing the nozzle diameter leads to an increase in process forces. A larger nozzle diameter results in higher gas flow rates and more efficient cooling. This phenomenon is attributed to the effective heat dissipation during roughing, resulting in raised cutting forces. Surprisingly, in finishing operations, increasing the nozzle diameter leads to a reduction in process forces. The finishing zone consists of both austenitic and martensitic regions (see Fig. 6), which are influenced by the prior martensite formation during roughing. A smaller nozzle diameter enhances local cooling, thereby increasing the force required for material separation during finishing.

THIS effect of nozzle diameter on process forces is particularly pronounced in turning without pre-cooling. Without pre-cooling, a smaller nozzle diameter results in significantly higher process forces during finishing. However, pre-cooling with LN_2 mitigates this effect by reducing the process forces.A possible hypothesis is that a smaller nozzle diameter leads locally to a stronger cooling of the component edge zone, whereby the forces increase accordingly. However, if the component has already cooled down to -72 °C, this effect decreases. Accordingly, the process forces also decrease. Another hypothesis could be that the geometry of the component changes with the temperature. The diameter of the sample shrinks with lower temperature and thus also the depth of cut in the process. This leads to different cutting depths depending on the prevailing component temperature. However, further investigations are needed in future work to explain this effect.

Finally, investigations were carried out using different workpiece batches. The batches examined differ in terms of chemical composition. Among other parameters, process forces were recorded, revealing an influence from the different workpiece batches on the process forces. In particular, the passive forces showed a scattering of approximately 60 N, while the other force components exhibited less variation, see Fig. 13. These findings are crucial to consider during dynamic pre-control for the targeted adjustment of martensite content.

For functional components that are exposed to very high mechanical loads during later use, very strict roughness requirements are placed on the component surface. Although the surface topography may appear similar across various cooling strategies at first glance (see Fig. 14), a detailed investigation reveals distinct differences contingent on the cooling approach. Turning without cooling exhibited an average surface roughness Rz of 3.1 µm after the finishing process. In contrast, the implementation of cooling strategies led to a notable reduction in surface roughness, with values as low as 2.6 µm.

a) Mass fraction in % of different batches

	Batch 1	Batch 2	Batch 3
Co	0.141	0.128	0.141
V	0.065	0.072	0.065
C	0.024	0.028	0.035
Si	0.268	0.429	0.380
Mn	1.57	1.90	2.00
Cr	18.44	18.24	18.39
Mo	0.416	0.406	0.238
Ni	7.85	7.95	8.16
N	0.079	0.093	0.086
P	0.017	0.008	0.011
S	0.020	0.005	0.017
Cu	0.652	0.399	0.403
Nb	0.027	0.005	0.004
Ti	0.010	0.001	0.001
Fe	70.29	70.25	69.93

(elements with mass fraction < 0.01 % in all three batches are not listed)

b) Process forces for the different batches

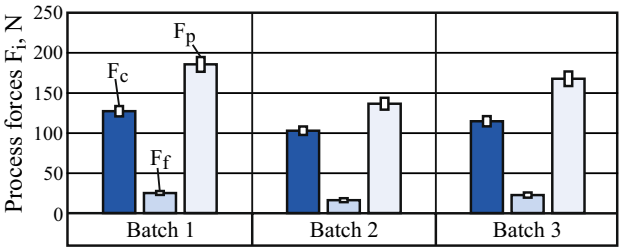

Roughing parameters:

v_c	= 100 m/min	tool: CNMG120412	
a_p	= 0.2 mm	material: 1.4301	
f	= 0.4 mm	cooling strategy: LN_2	

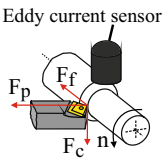

Fig. 13 **a** Mass fractions of different batches and **b** Influence of different batches on process forces

Looking additionally at the associated probability distributions, differences with regard to stochastic roughness are evident.

Comparing the surface topographies between roughing and finishing processes reveals significant differences, see Fig. 15. The finishing process demonstrates remarkable efficacy in reducing the average surface roughness Rz by a factor of six when compared to roughing. This improvement in surface quality is a desirable outcome for high-load functional components. While the two-step machining process significantly enhances surface quality, there is an important consideration regarding the induced martensite content. The finishing operation results in a loss of the induced martensite content introduced during the preceding roughing process. Future research in this area could explore innovative methods to preserve the induced martensite content during finishing, while maintaining superior surface quality, when LN_2 pre-cooling is used. Understanding the relationship between the machining process, surface topography, and the

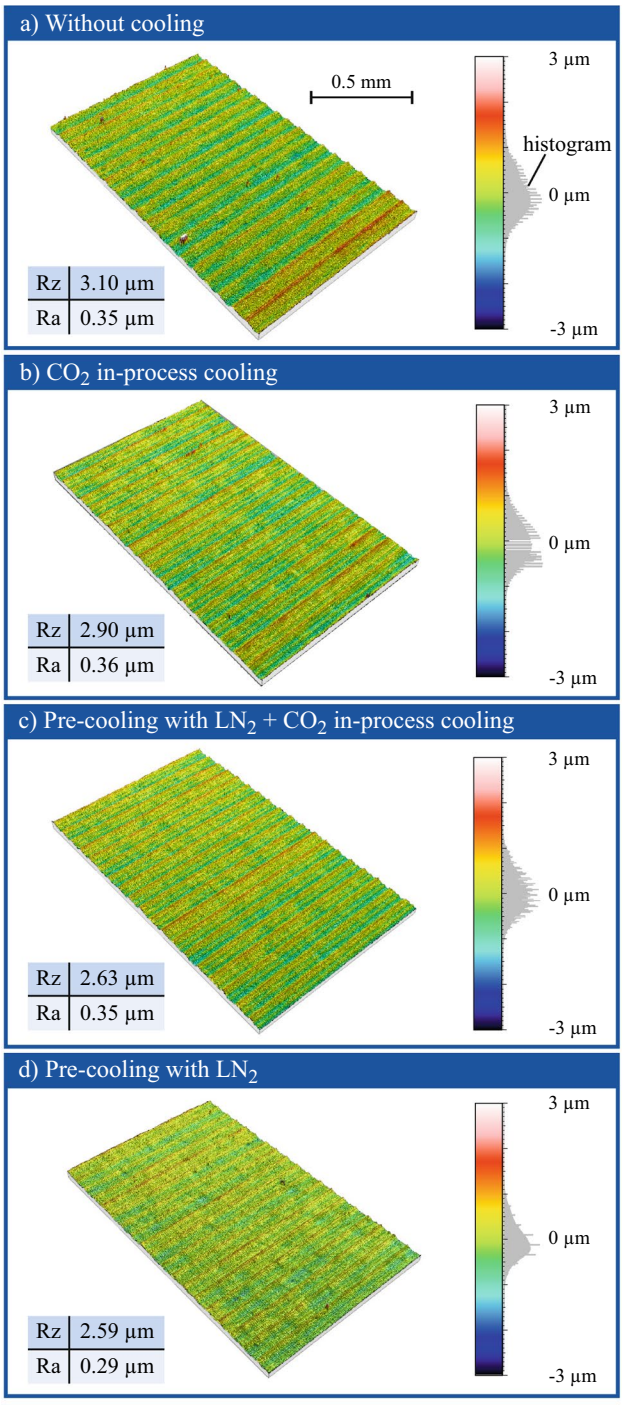

Fig. 14 Influence of different cooling strategies on surface topography

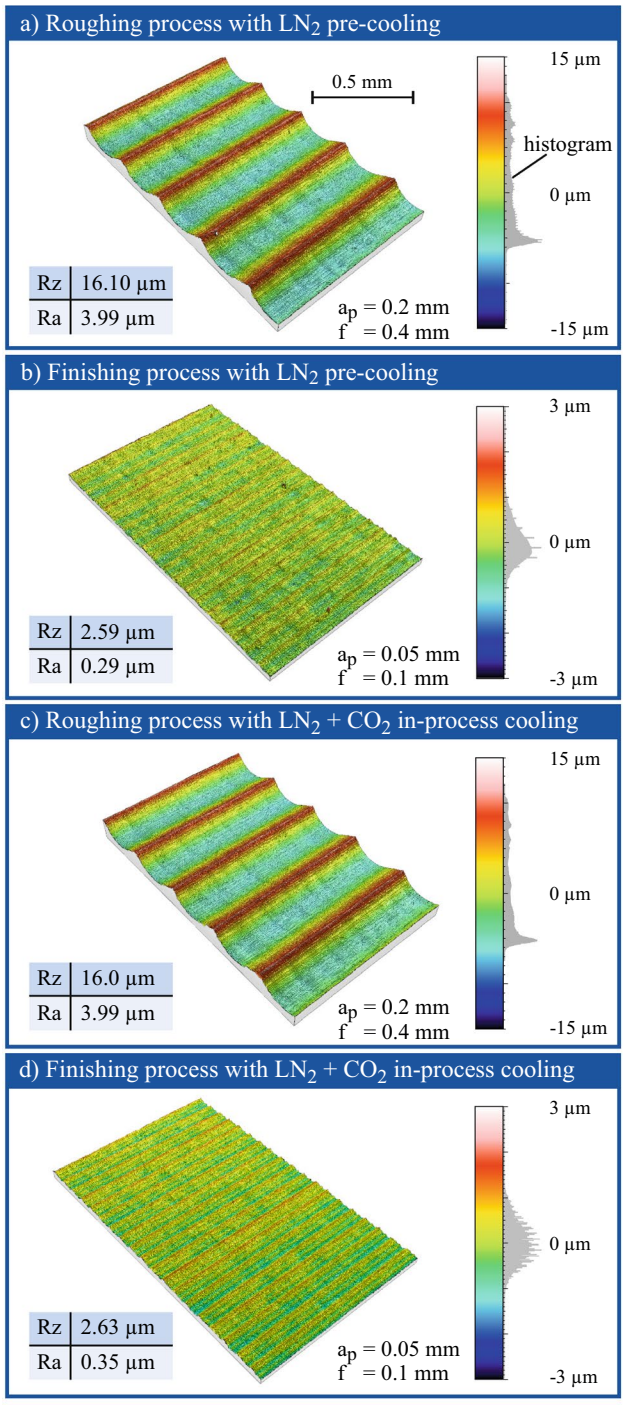

Fig. 15 Influence of different cooling strategies on surface topography

material's microstructure will further enhance the design and performance of functional components in demanding applications.

4.4 Numerical analysis of the temperature distribution

The first simulation results are shown in Fig. 16. The initial temperature of the component during turning (Fig. 16 a) and 16 b)) and the CO_2 nozzle diameter (Fig. 16 c)) were varied. The temperature distribution during conventional turning, without cooling, is shown in Fig. 16 a). Here, the influence of the tool cutting edge on the temperature in the separating zone is assumed with an equivalent power source in the form of a moving heat source. Here, maximum temperatures occur directly in the contact zone between the component surface and the indexable insert, with a rapidly decreasing gradient into the interior of the component. Pre-cooling with LN_2 leads to a significant reduction of the maximum temperatures occurring at the component surface by approx. 100 K. In addition, the surface that has already been machined quickly heats up to −15°C, while the starting temperature of −70°C is maintained inside the component. As it can be seen in Fig. 7, this cooling is sufficient to suppress the formation of white etching layers.

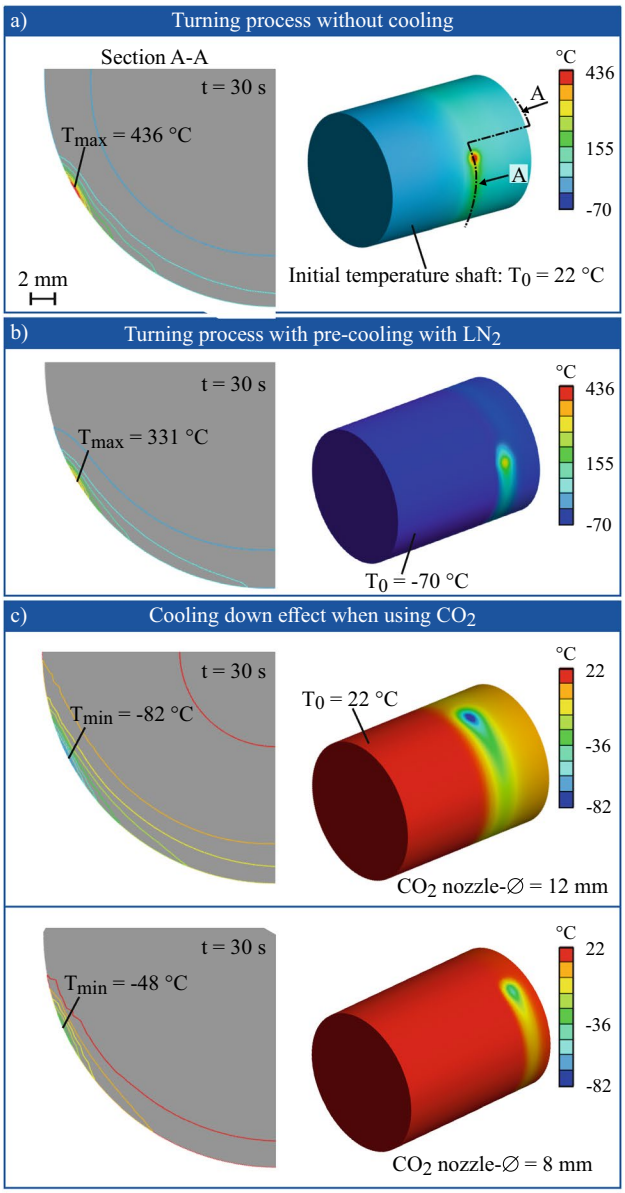

Fig. 16 The temperature distribution depending on different cooling strategies

In the next step, the isolated influence of CO_2 cooling on the workpiece temperature, without concurrent turning, was investigated (see Fig. 16 c)). The nozzle diameter was varied to analyze its effect on the formation of maximum surface temperatures and temperature distribution within the workpiece. Increasing the nozzle diameter from 8 mm to 12 mm resulted in a significant reduction of temperature at the workpiece surface, where the cooling jet impinges. Specifically, a temperature minimum of approximately −80°C was achieved at the workpiece surface with a nozzle diameter of 12 mm. However, this temperature minimum was localized and increased to room temperature within a few micrometers towards the inner region of the workpiece. Combining CO_2 cooling with LN_2 pre-cooling of the workpiece to −70°C did not lead to a significant increase in martensite content. This is lack of significant increase because the temperature difference between the initial surface temperature of the workpiece and the additional cooling provided by CO_2 was not sufficiently high. Furthermore, due to the short cooling time during the process (feed rate f = 0.4 mm and cutting speed v_c = 100 m/min), only surface cooling is achieved, and cooling within the inner regions of the workpiece is not feasible. Consequently, the implementation of CO_2 cooling during the process is only effective in keeping the martensite transformation constant for longer cutting paths, see also Fig. 5. This can be beneficial or be useful for reducing or preventing the rise in workpiece subsurface temperature due to convection and radiation with the ambient atmosphere.

4.5 Setting of the subsurface through process parameter selection

Apart from the workpiece geometry, its functionality can be set by a targeted modification of the subsurface with appropriate process parameters in the machining process. In addition to the hardening through deformation-induced martensite formation in the machining process, the surface

roughness also influences the workpiece properties. Thus, tailored machining, with differently required surface and subsurface properties, can be carried out if the corresponding process parameters are determined in such a way that desired target values are achieved. This can be used as the basis for an in-process control.

The Adaboost regressor for modeling the martensite content showed in pre-studies the best results compared with other regression model approaches, with a coefficient of determination $R^2 = 0.89$, an adjusted coefficient of determination $R^2_{adj} = 0.87$, and a root mean square error RMSE = 0.5. Varying the hyperparameters showed little effect on the model performance. The default values of the hyperparameters $n_{estimators} = 9$ and $random_{state} = 0$ were found to be the most appropriate for modeling the martensite formation.

For the surface roughness, the average peak to valley height Rz (DIN EN ISO 4287 [33]) was considered. The Pearson correlation coefficients show a strong influence of the feed on the roughness with 0.99, while the other process parameters have a low correlation. Therefore, the linear regression approach was chosen for modeling the roughness Rz with the feed as the only influencing process parameter. By this, a coefficient of determination of $R^2 = 0.92$, an adjusted coefficient of determination $R^2_{adj} = 0.90$, and a RMSE = 2.7 µm was achieved.

Using the objective function Z, the found process parameter combination was evaluated and optimized (2). In this case, the GA solves a minimization problem. The goal is to find process parameters with which the predicted target variables M_{Pred} and Rz_{Pred} (determined from the Adaboost model) are close to the given target values M_{Target} and Rz_{Target} to be achieved. Absolute differences are considered so that the deviation remains exclusively in the positive range. Via the weights w1 and w2, the importance of the target values can be weighted during the optimization process. These must add up to one again (3).

$$Z = w1 \cdot \mathrm{abs}(M_{Target} - M_{Pred}) + w2 \cdot \mathrm{abs}(Rz_{Target} - Rz_{Pred}) \quad (2)$$

$$w1 + w2 = 1 \quad (3)$$

Three different target values for the relative martensite content M were selected to test the method: M = 3, M = 4, and M = 5. The relative martensite content is a relative value, thus it does not have a unit. This has the advantage that the exact amount of martensite content does not have to be determined. For this, the measurement value of one sample was set as reference sample. The measurement values of the other samples are then linked relatively to this reference sample. A relative martensite content of e.g., M = 3 means that the measured signal of this sample is three times higher than the reference sample. The roughness was set to Rz = 10 µm and Rz = 30 µm. The weights w1 and w2 are set to w1 = 0.99 (and w2 = 0.01) and w1 = 0.6 (and w2 = 0.4). The weights were chosen to focus on martensite transformation in the first setup. In the second setup, the weight for surface roughness w2 is increased to focus more on the roughness in the optimization process. Through its significance, only feed f and workpiece pre-cooling temperature T are the variable process parameters, while the depth of cut ($a_p = 0.2$ mm) and cutting speed ($v_c = 70$ m/min) are fixed. The range of possible solution is limited from 0.1 mm to 0.5 mm for f and from −150°C to −50°C for T. The result diagrams for the adjustment tests are shown in Fig. 17 (for

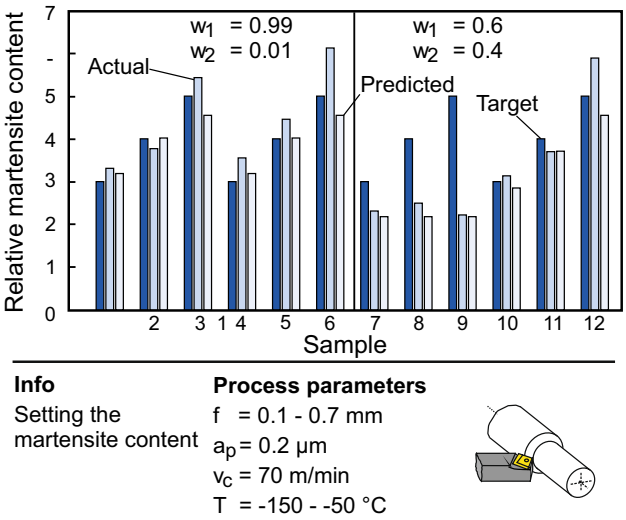

Fig. 17 Results for setting different martensite contents

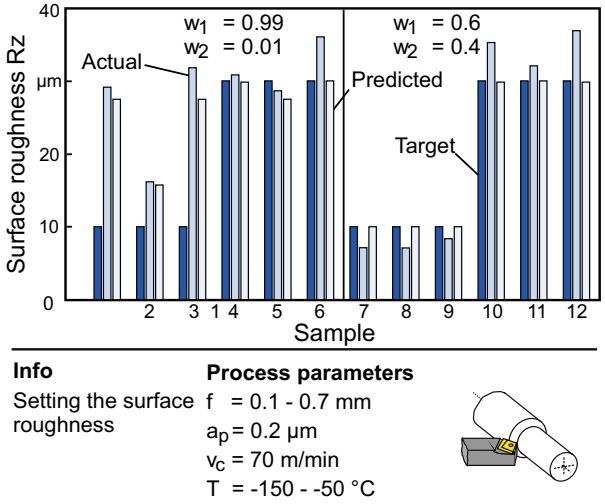

Fig. 18 Results for setting different surface roughnesses

Table 1 Percentage deviation for setting different martensite contents and surface roughnesses

Samples	Weight w1	Percentage deviation: Relative martensite content M			Percentage deviation: Surface roughness Rz		
		Actual/Target	Predicted/Target	Predicted/Actual	Actual/Target	Predicted/Target	Predicted/Actual
1	0.99	10.3	6.3	3.6	191.4	174.8	5.7
2	0.99	5.7	0.5	6.6	61.6	57.2	2.7
3	0.99	8.6	9.0	16.2	217.9	174.8	13.6
4	0.99	18.4	6.3	10.2	2.8	0.6	3.2
5	0.99	11.5	0.5	9.9	4.6	8.4	4.0
6	0.99	22.5	9.0	25.7	20.1	0.0	16.8
7	0.6	22.9	27.3	5.7	28.8	0.0	40.4
8	0.6	37.6	45.5	12.7	29.0	0.0	40.9
9	0.6	55.6	56.4	1.7	16.4	0.0	19.6
10	0.6	4.5	5.0	9.1	17.5	0.6	15.4
11	0.6	7.5	7.3	0.3	6.9	0.0	6.4
12	0.6	17.8	9.0	22.8	22.9	0.6	19.1
Mean	Total	18.6	15.2	10.4	51.7	34.7	15.6
Median	Total	14.6	8.1	9.5	21.5	0.6	14.5
Mean	0.99	12.8	5.3	12.0	83.1	69.3	7.7
Median	0.99	10.9	6.3	10.0	40.9	32.8	4.9
Mean	0.6	24.3	25.1	8.7	20.3	0.2	23.6
Median	0.6	20.4	18.2	7.4	20.2	0.0	19.3

martensite formation) and in Fig. 18 (for roughness). A distinction is made between target, predicted, and actual measured values after machining. The percentage deviations between those are also summarized in detail in table 1. The distinction between the percentage deviation between actual and target value allows to evaluate the performance of the whole method. The deviation between predicted and target values is good to evaluate the performance of the GA while the deviation between predicted and actual shows the deviations for the Adaboost model. The samples 1–6 include all possible target value combinations of martensite and roughness for the first setup (w1 = 0.99 and w2 = 0.01), while the samples 7–12 include the experiments for the second setup (w1 = 0.6 and w2 = 0.4).

For higher roughness target values (Rz = 30 µm), the algorithm was able to find suitable process parameters with which the target value specifications of both target variables were met. At the lower roughness target value (Rz = 10 µm), it is no longer possible to achieve the target values for both martensite content and roughness simultaneously. In this range, the conflict between the two target variables results from its opposite course due to the feed variation: A higher feed results in a higher martensite content, but also in a higher roughness. Hence, depending on the choice of the weights w1 and w2 in the objective function, the correspondingly higher weighted objective variable is taken into account more strongly in the selection of the process parameters. For example, it can be seen that for w1 = 0.99 (higher weighting for martensite formation than for roughness), the difference between target and modelled martensite content, resulting from the determined process parameters, is small (samples 1–3 in Fig. 17). In contrast, the other target value roughness cannot be achieved, which shows a high deviation between the target value and the predicted value (samples 1–3 in Fig. 18). In contrast, the higher weighting for the roughness with w1 = 0.6 shows the opposite (samples 7–9 in Fig. 17 and Fig. 18). This can also be seen in table 1, if the mean and median values of the percentage deviation between actual and target values for the weight w1 = 0.99 and w1 = 0.6 are compared with each other. Here, it becomes apparent that the temperature variation alone is not sufficient for higher required martensite content and an additional adjustment of the feed is necessary. However, this is limited in the lower feed range by the greater consideration of the roughness. This results in an increasing deviation between the target and the predicted value as the target martensite content increases (samples 7–9 in Fig. 17). Consequently, the conflict between the two target values becomes particularly apparent at target values for low roughness. At higher roughness target values (Rz = 30 µm), the target conflict is not significant, even with a higher weighting in favor of roughness (samples 10–12 in Fig. 18). Thus, these results confirm the need for a two-step turning process as well,

if apart from different martensite content, low roughness values are also required.

4.6 Feed forward control

The objective of the control concept proposed in this paper is the reliable adjustment of the martensite content of the machined surface. While a process parallel measurement of the martensite content is possible, a process parallel feedback control of the martensite content is not suitable, since the local martensite content is determined during the process, and the delay time of the control would result in remaining local deviations of the martensite content. Thus, a cross process control is needed. Due to the material expenditure and process time, the required result has to be achieved process-reliably with a minimum number of cuts. That is why a simple cross process feedback control is not suitable either. Furthermore, the resulting martensite content depends non-linearly on both feed and temperature, wherefore a model of these dependencies to choose the process parameters is required.

Since deviations occur between different workpieces, e.g.,, because of different batches or slight variations of the workpiece temperature, the model-based setting of the process parameters in an open loop system is not suitable either. Therefore, the feed forward control of the martensite content, shown in Fig. 19 was developed. While in principle both workpiece temperature T and feed f could be used as manipulated variables, the feed is chosen since it can be easily and precisely lowered and increased via the NC-control of the machine. Since the workpiece temperature still acts as a disturbance, it is measured for each cut and taken into account in the feed forward control. For this control, the model described in 4.5 is adapted to consider both, the deviation between the set martensite content M_{set} and the actual martensite content M_{act}, as well as the current temperature of the workpiece. This way, the actual martensite content is determined within the process using the eddy current sensor.

The communication with the machine and the data collection require a frequent actualisation in fixed intervals, while a recalculation of the manipulated variable is only necessary if the next cut has to be started. Furthermore, the computation time of the model, which is much longer than the cycle time suitable for the communication with the machine, had to be considered. Thus, the control is divided in a cycle oriented part and an event triggered part with calculation of the feed as the manipulated variable. The cycle oriented part contains the actual monitoring of the process, especially the collection of the sensor data and the communication with the machine via the PROFIBUS interface. Synchronous variables in the NC-Code are used to transmit the beginning, number and the end of each cut from the machine to the PLC, and to set the required feed as the manipulated variable. Currently the target martensite content of the control is constant over the machining length. Here, in principle, the setting of a local varied martensite content is also possible, especially if no in-process cooling method is applied. Hence, the mean value of the martensite content over the machining length is used as the controlled variable. In future applications, due to the in-process eddy current testing, even a defined set of a position dependent martensite content over the workpiece length might be possible.

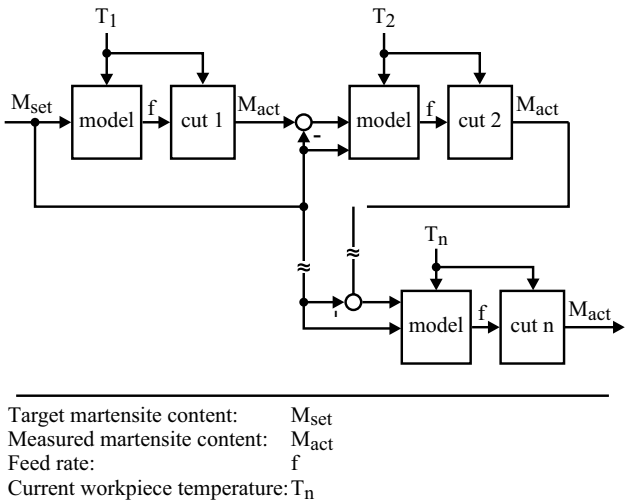

Fig. 19 Feed forward control concept

5 Conclusion

In this study, the influence of different cooling strategies on mechanical load and martensite transformation, during roughing and finishing turning operations, has been thoroughly investigated by force and in-process eddy current measurements.

Using in-process eddy current measurements, it is possible to reliably determine the actual martensite subsurface content. This value is then used in the feed forward control to detect possible differences to the desired martensite subsurface content.

The cooling strategies of CO_2 in-process cooling, pre-cooling with LN_2, and their combination have been evaluated, along with measurements without cooling as a reference. The results demonstrate that the choice of cooling strategy has a significant impact on process forces, particularly affecting the passive and cutting forces, while the feed force shows minimal variation. LN_2 pre-cooling exhibits a remarkable reduction in process forces compared to other cooling strategies, potentially attributable to altered chip formation. The cooling strategy also shows

an influence on the martensitic transformation. As it can be detected within the cutting process by eddy current testing, if no in-process cooling is applied, the martensite subsurface content decreases over the sample length. However, using LN_2 pre-cooling, higher subsurface martensite contents can be produced.

Moreover, the present study explores the impact of nozzle diameter on process forces during CO_2 in-process cooling. Increasing the nozzle diameter during roughing led to higher process forces, while in finishing, larger nozzle diameters resulted in reduced process forces. The interaction between prior martensite formation during roughing and cooling during finishing, affect the force distribution during the turning process. The cooling is sufficient to suppress the formation of white etching layers in the newly created subsurface. However, a formation of white etching layers inside cutting chips is observed.

The research also provides an insight into the surface topography of functional components subjected to high mechanical loads. Cooling strategy has been found to significantly influence the surface roughness, with cooling leading to reduced roughness values. The use of a two-stage machining process, comprising roughing and finishing, improved surface quality, but led to a reduction in induced martensite content due to the finishing operation. Future research should focus on innovative methods to preserve induced martensite content during finishing without compromising surface quality. This may involve optimizing the cooling process to achieve both desired surface roughness and an increased martensite content. Additionally, the impact of cooling strategies on chip morphology and phase transformations within the workpiece merits further exploration. A comprehensive understanding of these relationships will facilitate the development of tailored cooling approaches for specific applications, thereby enhancing the design and performance of functional components under demanding mechanical conditions.

Furthermore, workpiece temperature significantly influences martensite formation during machining. Simulation methods have been used to understand the temperature distribution inside the workpiece, in particular the impact of CO_2 cooling and nozzle diameter. The combination of CO_2 and prior nitrogen cooling has not been found to significantly increase martensite content. However, CO_2 cooling shows promise in increasing martensite transformation for longer cutting paths. For this purpose, further simulative investigations are required with regard to the temperature distribution in the component subsurface during the superposition of the heat, as well as the usage of a cold source as analogy for the in-process CO_2 cooling during the turning process. Further research can explore optimized cooling strategies to enhance martensite content and improve machining performance for high-load functional components.

The main objective of this work is to achieve a dynamic feed forward control for a targeted adjustment of the martensite content. Therefore, the actual martensite content can be detected by in-process eddy current testing. An inverse modeling approach is introduced to set the subsurface properties based on the appropriate choice of process parameters. In further investigations, the robustness of the control against various disturbances, e.g., due to workpieces from different batches, has to be investigated. Also, the minimum number of cuts to reliably achieve the desired martensite content is to be investigated. While currently, a constant martensite value over the cutting length is used as both an input value and output value, the generation of surfaces with varying surface properties over the workpiece length should be especially taken into account. In this case, in-process monitoring of the actual martensite subsurface content by eddy current testing becomes crucial. For a position-dependent martensite subsurface content, a variation of the feed, depending on the tool position and eddy current testing measurement results, is necessary.

Funding Open Access funding enabled and organized by Projekt DEAL. The scientific work has been supported by the Deutsche Forschungsgemeinschaft (DFG) within the research priority program SPP 2086 (grant project number 401800578). The authors thank DFG for funding.

Availability of data and materials Data is available from the corresponding author upon request.

Declarations

Conflict of interest The authors have no competing interests to declare that are relevant to the content of this article.

Ethical approval Not applicable.

Consent to participate Not applicable.

Consent for publication Not applicable.

References

1. Karpuschewski B, Kinner-Becker T, Klink A, Langenhorst L, Mayer J, Meyer D, Radel T, Reese S, Sölter J (2022) Process signatures-knowledge-based approach towards function-oriented manufacturing. Proc CIRP 108:624–629. https://doi.org/10.1016/j.procir.2022.01.001. (**6th CIRP Conference on Surface Integrity**)
2. Schwalm J, Gerstenmeyer M, Zanger F, Schulze V (2020) Complementary machining: effect of tool types on tool wear and surface integrity of AISI 4140. Proc CIRP 87:89–94. https://doi.org/10.1016/j.procir.2020.02.035. (**5th CIRP Conference on Surface Integrity (CSI 2020)**)
3. Stampfer B, González G, Gerstenmeyer M, Schulze V (2021) The present state of surface conditioning in cutting and grinding. J Manuf Mater Proces 5(3):1–17. https://doi.org/10.3390/jmmp5030092
4. Totten GE (ed) (2007) Steel heat treatment handbook, 2nd edn. CRC Taylor & Francis, Boca Raton
5. Frölich D, Magyar B, Sauer B, Mayer P, Kirsch B, Aurich JC, Skorupski R, Smaga M, Beck T, Eifler D (2015) Investigation of wear resistance of dry and cryogenic turned metastable austenitic steel shafts and dry turned and ground carburized steel shafts in the radial shaft seal ring system. Wear 328–329:123–131. https://doi.org/10.1016/j.wear.2015.02.004
6. Fricke LV, Nguyen HN, Breidenstein B, Denkena B, Dittrich MA, Zaremba D, Maier HJ (2020) Generation of tailored subsurface zones in steels containing metastable austenite by adaptive machining and validation by eddy current testing. Tech Mess 87(11):704–713
7. Fricke LV, Nguyen HN, Breidenstein B, Zaremba D, Maier HJ (2020) Eddy current detection of the martensitic transformation in AISI304 induced upon cryogenic cutting. Steel Res Int 92(1):2000299
8. Fricke LV, Nguyen HN, Appel J, Breidenstein B, Maier HJ, Zaremba D, Barton S (2022) Characterization of deformation-induced martensite by cryogenic turning using eddy current testing. Proc CIRP 108:49–54. https://doi.org/10.1016/j.procir.2022.03.014. (**6th CIRP Conference on Surface Integrity**)
9. Fricke LV, Thürer SE, Jahns M, Breidenstein B, Maier HJ, Barton S (2022) Non-destructive, contactless and real-time capable determination of the α′-martensite content in modified subsurfaces of AISI 304. J Nondestruct Eval 41(4):123. https://doi.org/10.1007/s10921-022-00905-x
10. Denkena B, Breidenstein B, Dittrich MA, Nguyen HN, Fricke LV, Maier HJ, Zaremba D (2021) Effects on the deformation-induced martensitic transformation in AISI 304 in external longitudinal turning. Adv Ind Manuf Eng 2:100044. https://doi.org/10.1016/j.aime.2021.100044
11. Denkena B, Breidenstein B, Dittrich MA, Wichmann M, Nguyen HN, Fricke LV, Zaremba D, Barton S (2022) Setting of deformation-induced martensite content in cryogenic external longitudinal turning. Proc CIRP 108:170–175. https://doi.org/10.1016/j.procir.2022.03.030. (**6th CIRP Conference on Surface Integrity**)
12. Kirsch B, Hotz H, Müller R, Becker S, Boemke A, Smaga M, Beck T, Aurich JC (2019) Generation of deformation-induced martensite when cryogenic turning various batches of the metastable austenitic steel AISI 347. Prod Eng Res Devel 13:343–350. https://doi.org/10.1007/s11740-018-00873-0
13. Aurich JC, Mayer P, Kirsch B, Eifler D, Smaga M, Skorupski R (2014) Characterization of deformation induced surface hardening during cryogenic turning of AISI 347. CIRP Ann 63(1):65–68. https://doi.org/10.1016/j.cirp.2014.03.079
14. Mayer P, Kirsch B, Müller C, Hotz H, Müller R, Becker S, von Harbou E, Skorupski R, Boemke A, Smaga M, Eifler D, Beck T, Aurich JC (2018) Deformation induced hardening when cryogenic turning. CIRP J Manuf Sci Technol 23:6–19. https://doi.org/10.1016/j.cirpj.2018.10.003
15. Bartarya G, Choudhury SK (2012) Effect of Cutting Parameters on Cutting Force and Surface Roughness During Finish Hard Turning AISI52100 Grade Steel. Procedia CIRP. 1:651–656. https://doi.org/10.1016/j.procir.2012.05.016. (**Fifth CIRP Conference on High Performance Cutting 2012**)
16. Rao CJ, Rao DN, Srihari P (2013) Influence of cutting parameters on cutting force and surface finish in turning operation. Proc Eng 64:1405–1415. https://doi.org/10.1016/j.proeng.2013.09.222. (**International Conference on Design and Manufacturing (IConDM2013).**)
17. Hotz H, Smaga M, Kirsch B, Zhu T, Beck T, Aurich JC (2020) Characterization of the subsurface properties of metastable austenitic stainless steel AISI 347 manufactured in a two-step turning process. Proc CIRP 87:35–40. https://doi.org/10.1016/j.procir.2020.02.012. (**5th CIRP Conference on Surface Integrity (CSI 2020)**)
18. Fricke LV, Basten S, Nguyen HN, Breidenstein B, Kirsch B, Aurich JC, Zaremba D, Maier HJ, Barton S (2023) Combined influence of cooling strategies and depth of cut on the deformation-induced martensitic transformation turning AISI 304. J Mater Process Technol 312:117861. https://doi.org/10.1016/j.jmatprotec.2023.117861
19. Kirsch B, Basten S, Hasse H, Aurich JC (2018) Sub-zero cooling: A novel strategy for high performance cutting. CIRP Ann 67(1):95–98. https://doi.org/10.1016/j.cirp.2018.04.060
20. Basten S, Kirsch B, Hasse H, Aurich JC (2019) Turning of AISI 4140 (42CrMo4): a novel sub-zero cooling approach. In: Schmitt R, Schuh G (eds) Advances in production research. Springer International Publishing, Cham, pp 313–323
21. Böß V, Denkena B, Breidenstein B, Dittrich MA, Nguyen HN (2019) Improving technological machining simulation by tailored workpiece models and kinematics. Proc CIRP 82:224–230. https://doi.org/10.1016/j.procir.2019.04.157. (**17th CIRP Conference on Modelling of Machining Operations**)
22. Fricke LV, Gerstein G, Kotzbauer A, Breidenstein B, Barton S, Maier HJ (2022) High strain rate and stress-state-dependent martensite transformation in AISI 304 at low temperatures. Metals. https://doi.org/10.3390/met12050747
23. Olson GB, Cohen M (1972) A mechanism for the strain-induced nucleation of martensitic transformations. J Less Common Metals 28(1):107–118
24. Maxwell PC, Goldberg A, Shyne JC (1974) Stress-assisted and strain-induced martensites in Fe-Ni-C alloys. Metall Trans 5(6):1305–1318
25. Fricke LV, Gerstein G, Breidenstein B, Nguyen HN, Dittrich MA, Maier HJ, Zaremba D (2021) Deformation-induced martensitic transformation in AISI304 by cryogenic machining. Mater Lett 285:129090. https://doi.org/10.1016/j.matlet.2020.129090
26. Akcan S, Shah W, Moylan S, Chandrasekar S, Chhabra P, Yang H (2002) Formation of white layers in steels by machining and their characteristics. Metall and Mater Trans A 04(33):1245–1254. https://doi.org/10.1007/s11661-002-0225-z
27. Souza P, Cangussu V, Câmara M, Abrao A, Denkena B, Breidenstein B, Meyer K (2020) Formation of white etching layers by deep rolling of AISI 4140 steel. J Mater Eng Perform 07(29):4351–4359. https://doi.org/10.1007/s11665-020-04988-3
28. Hossain R, Pahlevani F, Witteveen E, Banerjee A, Joe B, Prusty BG, Dippenaar R, Sahajwalla V (2017) Hybrid structure of white layer in high carbon steel—formation mechanism

and its properties. Sci Rep 7:13288. https://doi.org/10.1038/s41598-017-13749-7
29. González G, Sauer F, Plogmeyer M, Gerstenmeyer M, Bräuer G, Schulze V (2022) Effect of thermomechanical loads and nanocrystalline layer formation on induced surface hardening during orthogonal cutting of AISI 4140. Proc CIRP 108:228–233. https://doi.org/10.1016/j.procir.2022.03.040
30. Guo YB, Sahni J (2004) A comparative study of hard turned and cylindrically ground white layers. Int J Mach Tools Manuf 44(2):135–145. https://doi.org/10.1016/j.ijmachtools.2003.10.009
31. Iynen O, Eksi AK, Özdemir M, Akyildiz HK (2021) Experimental and numerical investigation of cutting forces during turning of cylindrical AISI 4340 steel specimens. Mater Test 63(5):402–410. https://doi.org/10.1515/mt-2020-0069
32. Olson GB, Cohen M (1976) A general mechanism of martensitic nucleation: part II. FCC → BCC and other martensitic transformations. Metall Trans A. 7(12):1905–1914. https://doi.org/10.1007/BF02659823
33. Deutsches Institut für Normung.: Geometrical Product Specifications (GPS) - Surface texture: profile method—Terms, definitions and surface texture parameters. DIN EN ISO 4287:2010-07